*Article*

# Empirical Failure Pressure Prediction Equations for Pipelines with Longitudinal Interacting Corrosion Defects Based on Artificial Neural Network

Suria Devi Vijaya Kumar *[iD], Michael Lo [iD], Saravanan Karuppanan [iD] and Mark Ovinis [iD]

Mechanical Engineering Department, Universiti Teknologi Petronas, Seri Iskandar 32610, Perak, Malaysia; michael_19000348@utp.edu.my (M.L.); saravanan_karuppanan@utp.edu.my (S.K.); mark_ovinis@utp.edu.my (M.O.)
* Correspondence: suria_19001431@utp.edu.my

**Abstract:** Conventional pipeline failure pressure assessment codes do not allow for failure pressure prediction of interacting defects subjected to combined loadings. Alternatively, numerical approaches may be used; however, they are computationally expensive. In this work, an analytical equation based on finite element analysis for the failure pressure prediction of API 5L X52, X65, and X80 corroded pipes with a longitudinal interacting corrosion defect subjected to combined loadings is proposed. An artificial neural network (ANN) trained with failure pressure obtained from finite element analysis (FEA) of API 5L X52, X65, and X80 pipes for varied defect spacings, depths and lengths, and axial compressive stress were used to develop the equation. Subsequently, a parametric study on the effects of the defect spacing, length, and depth, and axial compressive stress on the failure pressure of a corroded pipe with longitudinal interacting defects was performed to demonstrate a correlation between defect geometries and failure pressure of API 5L X52, X65, and X80 pipes, using the equation. The new equation predicted failure pressures for these pipe grades with a coefficient of determination ($R^2$) value of 0.9930 and an error range of $-10.00\%$ to $1.22\%$ for normalized defect spacings of 0.00 to 3.00, normalized effective defect lengths of 0.00 to 2.95, normalized effective defect depths of 0.00 to 0.80, and normalized axial compressive stress of 0.00 to 0.80.

**Keywords:** artificial neural network; failure pressure prediction; pipeline corrosion

## 1. Introduction

A pipeline is a critical steel structure that transports hydrocarbons efficiently and ensures energy security [1]. Pipelines are increasingly transitioning to high-strength steel, which significantly improves transportation efficiency and lowers installation costs. According to statistics, pipeline construction cost can be decreased by 7% for each grade improvement in steel strength [2]. As such, high-grade steel pipelines are becoming increasingly popular in the oil and gas industry [3]. However, when dealing with steel pipes, corrosion is a major issue, as it can result in catastrophic failures if not handled appropriately [4–7]. With the increase of high-grade steel pipeline usage, the need for reliable and efficient pipeline failure pressure assessment methods that cater for high-strength steel is necessary for safe operations.

Among various types of corrosion that occurs in hydrocarbon pipelines, localized corrosion is one of the most dangerous corrosion types, as the deterioration of the metal occurs in an accelerated manner [5]. This type of corrosion typically causes the cracking or perforation of a material, resulting in the rapid collapse of the structure. There are several forms of localized corrosion that are commonly found in oil and gas pipelines caused by various failure mechanisms. Among them, pitting corrosion is one of the most destructive forms of corrosion [6,7].

In a pristine pipe, the hoop stress is distributed evenly throughout the pipe. However, in the presence of internal and external corrosion defects, the hoop stress distribution is nonuniform [5,6]. In the region of defect, the deepest defect experiences the highest stress from the exertion of internal pressure on the pipe walls. Strain builds up at the region of defect when the pipeline is subjected to axial compressive stress, making it the most critical region in the pipeline [7]. Generally, corrosion assessment codes are used to assess the failure pressure of corroded pipelines in the industry. The ASME B31G, Modified ASME B31G, SHELL92, RSTRENG, and DNV-RP-F101 (DNV) are some of the conventional corrosion assessment codes used, as summarized in Table 1 [8–11].

**Table 1.** Conventional pipe failure pressure assessment codes [8–11].

| Method | Fundamental Equation | Governing Assumption | Material Restriction | Defect Idealization |
|---|---|---|---|---|
| ASME B31G | NG-18 | Failure pressure caused by flow-stress-dependent mechanism | Low toughness | Parabolic or rectangular |
| Modified B31G | NG-18 | | Low toughness | Mixed shape |
| SHELL 92 | NG-18 | | - | Rectangular |
| RSTRENG | NG-18 | | | Effective area |
| DNV RP-F101 | NG-18 | Pipe failure controlled by plastic flow (ultimate tensile strength is the flow stress) | Moderate toughness | Rectangular |

Among them, the DNV method is known to be the most comprehensive assessment code for the failure pressure of corroded pipes [12]. However, either the failure pressure assessment of a pipe with single corrosion defect subjected to internal pressure and axial compressive stress or with interacting defects subjected to internal pressure only is available [10]. In reality, pipelines are generally susceptible to interacting corrosion defects and are subjected to combined internal pressure and axial compressive stress loading [12,13]. Furthermore, applying the corrosion assessment codes to assess high-toughness pipelines will result in inaccurate failure pressure predictions, as these codes are recommended for low- to medium-toughness pipelines [6,10].

In recent years, machine learning has been researched to replace the time-consuming methods and conventional codes. The failure pressure predictions obtained by utilizing these tools are more accurate and less conservative compared to the conventional approaches [14]. Belachew et al., (2011) developed empirical equations for failure pressure prediction of corroded pipelines by investigating the influence of defect geometries on pipe failure pressure of an API 5L X52 pipe using the finite element method (FEM). They found that conventional corrosion assessment methods result in conservative failure pressure predictions [7]. Following this approach, Arumugam et al., (2020) [4], developed empirical equations for the failure pressure prediction of a medium-toughness API 5L X52 pipe with a single corrosion defect subjected to combined loadings by utilizing the Buckingham Pi theorem. They found that the proposed model resulted in more accurate predictions compared to the DNV method [4]. However, unlike the conventional codes, there were numerous equations, each for a specific range of parameters.

Lo et al., (2021) developed empirical equations for longitudinally interacting corrosion defects of API 5L X65 pipes subjected to combined loadings. Their study utilized an artificial neural network (ANN) for the development of the empirical equations. An ANN was trained using data generated using FEM. The proposed model was capable of predicting the failure pressures accurately with a coefficient of determination ($R^2$) value of 0.99 [5].

All these studies revealed the conservativeness of the DNV method. The DNV equations were derived based on a series of full-scale burst tests and finite element analysis (FEA) which were then reduced for practical applications. Thus, the failure pressure predic-

tions produced by DNV reflect an average or mean approximation of the burst capacity of corrosion-damaged pipelines. Additionally, its conservatism stems from the fact that it uses a material's ultimate tensile strength ($\sigma_{UTS}$) as the flow stress, rather than its true ultimate tensile strength ($\sigma_{UTS}^*$), even though materials fail when stresses exceed $\sigma_{UTS}^*$.

To overcome the limitations of the current codes, Silva et al., (2007) investigated the relationship between interacting corrosion defects and pipe burst pressure using FEA and ANN, with the FEA providing training data for the ANN. They found in their study that combining FEA with ANN for the purpose of assessing the structural integrity of corroded pipelines is a promising and efficient technology [15]. Xu et al. used this approach in 2017 to investigate the effect of corrosion defect geometry on the failure pressure of a corroded pipe by integrating FEA and ANN. They ensured the accuracy of their finite element model by using appropriate meshing and boundary conditions. The resulting FEA model accurately predicted failure pressures with a relative error of less than 1%, and their ANN model accurately predicted failure pressures of pipelines with interacting defects with a relative error of less than 2% [16]. However, they did not investigate the compressive stresses acting on the pipe during their research.

The development of a generalized empirical corrosion assessment method for the failure pressure prediction of single and interacting corrosion defects subjected to combined loading for pipe grades ranging from medium to high toughness is a challenge due to the complexity and multiple parameters to be considered during the assessment [17,18]. In the DNV code, the defect length, defect depth, defect width, defect spacing for interacting defects, axial compressive stress, and the ultimate tensile strength of the material are taken into account [10]. As mentioned earlier, despite being the most comprehensive assessment method in the industry, the DNV code is recommended for low- to medium-toughness pipes only. In addition, it is not applicable to interacting defects subjected to combined loadings.

By incorporating axial compressive stress acting on a pipe, Lo et al. [5] and Vijaya Kumar et al. [6] advanced their research in this area. In their investigation, they employed the created ANN to derive an empirical equation in matrix form. The equation was created as a function of the normalized axial compressive stress, the normalized defect depth, length, and spacing. Both experiments demonstrated that when compared to full-scale burst testing, the established equations could accurately predict the failure pressure of a corroded pipe with an error percentage of less than 5%.

Based on Table 2, to fill the void of the conventional assessment methods, this study proposes an empirical model for the failure pressure prediction of interacting defects in the longitudinal direction subjected to combined loadings for API 5L X52, X65, and X80 pipes (the most commonly used pipes in the industry).

**Table 2.** Summary of common corrosion assessment approaches.

| Method | Advantage | Limitation |
|---|---|---|
| DNV-RP-F101 (most comprehensive) | Most comprehensive code for low- to medium-toughness pipes | Conservative<br>Does not cater for interacting defects subjected to combined loading |
| Finite Element Method | Highly accurate<br>Caters for all material grades and defect orientation | Complex<br>Requires usage of software<br>Time-consuming |
| Artificial Neural Network | Able to process complex nonlinear data<br>Robust | Requires a large dataset for training and development |

An artificial neural network developed with training data obtained from finite element analysis (FEA) approach similar to that of Lo was adopted. The following are the main contributions of this study:

1. Development of failure pressure assessment method for medium- to high-toughness pipeline with longitudinally aligned interacting corrosion defects subjected to internal pressure and axial compressive stress.
2. Establishment of a correlation between defect geometry, axial compressive stress, and failure pressure of a medium- to high-toughness pipeline with longitudinally aligned interacting corrosion defects subjected to internal pressure and axial compressive stress.

## 2. Methodology

### 2.1. Development of the Artificial Neural Network

The first step in the development of the artificial neural network was to generate comprehensive training data for longitudinally aligned interacting corrosion defects subjected to internal pressure and axial compressive stress for pipe grades ranging from medium- to high-toughness materials. The second step involves training of the ANN, followed by validation of the model.

### 2.1.1. Generation of ANN Training Data

The training data for the ANN were generated using FEA for a range of parameters for API 5L X52, X65, and X80 pipe grades. The material properties are tabulated in Table 3 and the geometric parameters of the corroded pipe are tabulated in Table 4. The material properties of the pipe body are represented by a nonlinear true stress–strain curve of the materials during the finite element simulations, as illustrated in Figure 1. FEM has proven to be a reliable tool for structural analysis and many researchers have utilized this method to generate training data for the development of an ANN [5,19]. However, prior to the FEA, the FEM was validated against full-scale burst tests to ensure that the methodology and applied boundary conditions are correct.

**Table 3.** Material properties of the pipe grades used in this study [5,7,20].

| Properties | Pipe Body | | | Pipe End Cap |
|---|---|---|---|---|
| | API 5L X52 | API 5L X65 | API 5L X80 | |
| Modulus of elasticity, $E$ | | 210.0 GPa | | 200.0 TPa |
| Poisson's ratio, $v$ | | 0.3 | | 0.3 |
| Yield strength, $\sigma_y$ | 359.0 MPa | 464.0 MPa | 534.1 MPa | - |
| True ultimate tensile strength, $\sigma_{UTS}^*$ | 612.0 MPa | 629.0 MPa | 718.2 MPa | - |

**Table 4.** Geometric parameters of the corroded pipe models.

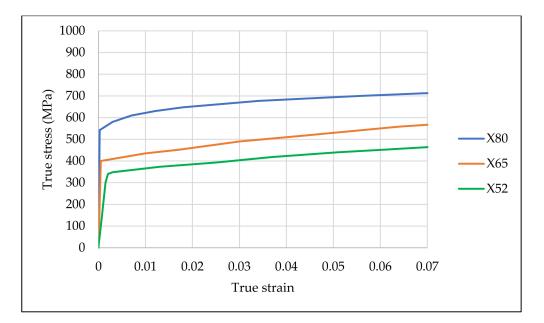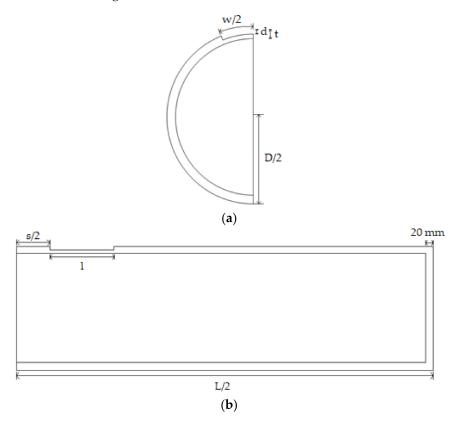| Input Parameters | Values |
|---|---|
| Outer diameter of pipe, $D$ (mm) | 300 |
| Length of pipe, $L$ (mm) | 2000 |
| Wall thickness, $t$ (mm) | 10 |
| Normalized defect width, $w/t$ | 10 |
| Normalized effective defect depth, $(d/t)_e$ | 0.00–0.80 |
| Normalized effective defect length, $(l/D)_e$ | 0.00–2.95 |
| Normalized longitudinal defect spacing, $s_l/\sqrt{Dt}$ | 0.0–3.00 |
| Normalized longitudinal compressive stress, $\sigma_c/\sigma_y$ | 0.00–0.80 |

**Figure 1.** True stress–strain curve for API 5L X52, X65, and X80 steel pipe [5,7,20].

In this study, quarter pipes with rectangular shape idealization of corrosion defects were modeled using AutoCAD. Quarter models reduce computation time while rectangular defect idealization allows for a safer, lower bound failure pressure prediction without compromising on accuracy [4,5,7,10,21]. The pipes were modeled with end caps for even distribution of axial compressive stress and the full length of the model was set to 2000 mm to eliminate end cap influence [4,5,7,10]. Figure 2 illustrates an example of the quarter model used during the FEA.



**(a)**



**(b)**

**Figure 2.** A quarter pipe model with longitudinally aligned interacting corrosion defects viewed from the (**a**) front (**b**) side.

Prior to the finite element simulations, the quarter models were meshed using AN-SYS 16.1 Structural Product of Mechanical ANSYS Parametric Design Language (APDL), referred to as ANSYS. Hexahedral SOLID185 (linear order) and tetrahedral SOLID186 (quadratic order) elements were used to mesh the pipe body and end cap, respectively [4,5,7,22]. These elements were used to represent the solid structure [23].

With a total of three layers and mesh size of 2 mm in length and depth, the mesh settings at the defect region were in line with the recommendations by the British Standards Institution (BSI) [24]. Prior to finalizing the mesh settings, a convergence test was carried out to optimize the number of elements to ensure minimum computation time without compromising accuracy. Moving away from the defect region, a mesh bias with an aspect ratio of 0.5 was applied to the elements with a total of 80 divisions. The details and results of the convergence test are presented in Table 5.

**Table 5.** Convergence test details and results.

| Number of Element Layers | Normalized Failure Pressure, $P_f/P_i$ |
| --- | --- |
| 1 | 0.92 |
| 2 | 0.93 |
| 3 | 0.95 |
| 4 | 0.95 |
| 5 | 0.95 |

Since quarter models were utilized in this study, symmetrical boundary conditions were applied to the model for the model to be treated as a whole pipe. Degree of freedom (DOF) in the $x$, $y$, and $z$ directions were constrained at 4/5 of the model length away from the region of interest. As for the applied loadings in this transient analysis, incremental ramped loading was used to apply internal pressure and axial compressive stress on the pipe walls [4,7]. The loadings were applied in two timesteps, first axial compressive stress, then internal pressure during the second timestep. The following assumptions were made during the FEA:

1. Isothermal condition (constant temperature throughout the simulation).
2. Isotropic and homogenous pipe model (uniform material properties in all directions).

The failure pressure was determined using von Mises yield criterion, where the pipe is said to have failed when the von Mises stress reaches the true ultimate tensile strength of the material [4,25,26]. As the defect region is the most critical part of the pipe, the von Mises stress is concentrated at this region (depicted by the red contour in Figure 3) and ultimately causes the pipe to fail when the stress penetrates throughout the wall thickness. In ANSYS, the von Mises stress is calculated as a function of hoop, radial, and axial stress. The timestep at which the effective stress equals to the true ultimate tensile strength of the material is used to determine the failure pressure of the pipe.

Before proceeding with the FEA, the FEM was validated against burst tests to ensure its accuracy and correct application of loads. Burst tests carried out by Bjorney et al. [27] and Benjamin et al. [28] were used to validate the method. The summary and results of the validation are presented in Tables 6 and 7. The greatest differences between the results obtained from FEM and burst tests were only 5.92% and 2.46% for single and interacting defects, respectively. Negative values indicate conservative predictions with the predicted pressure not exceeding the actual failure pressure. Hence, it is evident that the FEM is reliable to be used as a failure pressure data generation tool for the training of the ANN.
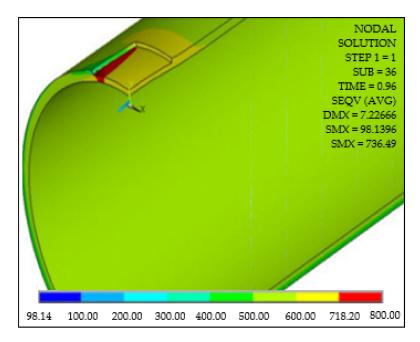
**Figure 3.** Illustration of the region of failure depicted by the red contour.

**Table 6.** Summary of burst test details by Bjorney et al. and Benjamin et al.

| Grade | Specimen | $d$ (mm) | $l$ (mm) | $w$ (mm) | $\sigma_l$ (MPa) | $s_l$ (mm) | $s_c$ (mm) |
|---|---|---|---|---|---|---|---|
| X52 [27] | Test 1 | 5.15 | 243 | 154.5 | 0.0 | - | - |
| | Test 5 | 3.09 | 162 | 30.9 | 48.0 | - | - |
| | Test 6 | 3.09 | 162 | 30.9 | 84.0 | - | - |
| X80 [28] | IDTS 2 | 5.39 | 39.6 | 31.9 | - | 0.0 | 0.0 |
| | IDTS 3 | 5.32 | 39.6 | 31.9 | - | 20.5 | 0.0 |
| | IDTS 4 | 5.62 | 39.6 | 32.0 | - | 0.0 | 9.9 |

**Table 7.** FEM validation against full scale burst tests by Bjorney et al. and Benjamin et al.

| Specimen | Burst Pressure (MPa) | FEA Failure Pressure (MPa) | Percentage Difference (%) |
|---|---|---|---|
| Test 1 | 23.2 | 22.95 | −1.08 |
| Test 5 | 28.6 | 28.35 | −0.87 |
| Test 6 | 28.7 | 27.00 | −5.92 |
| IDTS 2 | 22.68 | 22.40 | −1.23 |
| IDTS 3 | 20.31 | 20.12 | −0.94 |
| IDTS 4 | 21.14 | 20.62 | −2.46 |

2.1.2. Training of the Artificial Neural Network

MATLAB R2021b (MathWorks Inc., Natick, MA, USA) was used to develop a multi-layer feedforward neural network with Levenberg–Marquardt backpropagation algorithm, as illustrated in Figure 4. This algorithm falls under a supervised learning paradigm where the neural network is presented with a set of input parameters and the expected output [8,29]. This algorithm is a more efficient algorithm due to its second-order convergence rate, which requires lesser iterations.
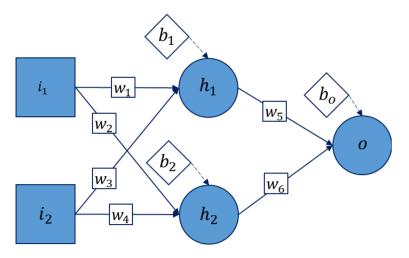
**Figure 4.** A simple multilayer feedforward neural network.

The input parameters of the model are the true ultimate tensile stress, normalized defect depth, length and spacing, and normalized axial compressive stress. The corresponding output of the ANN is the normalized failure pressure of the pipe was obtained using FEA. The failure pressure of the corroded pipes obtained using FEM was normalized using the intact pressure (Equation (1)) of the pipe before it was fed to the ANN for training [5,6,30].

$$P_i = \frac{\sigma^*_{UTS} t}{r_i} \tag{1}$$

The optimization of the neural network in terms of the number of hidden layers and neurons was based on a convergence test. The aim was to develop a neural network with the least number of neurons, as the complexity of the empirical equation increases with the number of neurons. The activation functions used are hyperbolic tangent function (Equation (2)) at the hidden layers and linear function (Equation (3)) at the output node.

$$a(x) = \frac{2}{1 + e^{-2x}} - 1 \tag{2}$$

$$f(x) = x \tag{3}$$

A total of 70% of the dataset was used for training the ANN, while 15% each of the remaining dataset were reserved as the validation and test dataset, to prevent overfitting [5,17,29]. The training process starts with the random initialization of the weights and biases of the ANN. After each iteration, the algorithm calculates the mean square error of the validation dataset. The iteration was stopped upon reaching the maximum number of epoch or validation checks. The weights and biases at the epoch that produces the best validation performance were chosen and applied to the ANN. The ANN was validated based on its ability to produce results close to the training data. This was measured using the coefficient of determination ($R^2$) value of the neural network with a value of 0.99 deemed acceptable.

## 2.2. Development of the Empirical Equation

The empirical equation was developed based on the weights and biases of the trained ANN. The entire neural network is represented by matrix equations, which become the basis of the developed corrosion assessment equations. Based on Figure 4, the neurons in the input layer ($i_x$) are connected to each neuron in the adjacent hidden layer ($h_x$) through synoptic weights ($w_x$). Every piece of information transferred from the input layer is multiplied with the corresponding synaptic weight and they are summed up. The summed product forms an input to an activation function ($a[x]$), and a bias value ($b_x$) is added to the result of the function. The new sum is then transferred to the neurons in the next hidden

layer and the process is repeated till it reaches the output neuron [16]. This process can be represented in matrix form as in Equations (4) and (5) [29].

$$
\begin{bmatrix} h_1 \\ h_2 \end{bmatrix} = \begin{bmatrix} w_1 & w_3 \\ w_2 & w_4 \end{bmatrix} \begin{bmatrix} i_1 \\ i_2 \end{bmatrix} + \begin{bmatrix} b_1 \\ b_2 \end{bmatrix} \tag{4}
$$

$$
[o] = \begin{bmatrix} w_5 & w_6 \end{bmatrix} \begin{bmatrix} a(h_1) \\ a(h_2) \end{bmatrix} + [b_o] \tag{5}
$$

During the training process, the inputs of the ANN are normalized to standardize the parameters and prevent dominance of inputs with large values. The input parameters and output of the developed equation have to be normalized and denormalized accordingly using Equations (6) and (7), respectively, as a min–max normalization, where a minimum and maximum value of $-1$ and $1$ were used.

$$
i_n = \frac{(i_{n,\,max} - i_{n,\,min})(i - i_{min})}{(i_{max} - i_{min})} + i_{n,\,min} \tag{6}
$$

$$
o = \frac{(o_n - o_{n,\,min})(o_{max} - o_{min})}{(o_{n,\,max} - o_{n,\,min})} + o_{min} \tag{7}
$$

## 3. Results

### 3.1. Development of Artificial Neural Network

A total of 1843 datasets were used to train the ANN. A convergence test was carried out to optimize the number of hidden layers and neurons to ensure that the complexity of the empirical equation is minimized. The outcome of the convergence test is tabulated in Table 8. As a result, an ANN with one hidden layer and seven neurons in the hidden layer was developed, as illustrated in Figure 5. With a maximum epoch number of 2000 and 1500 validation checks, 15% of the training dataset was reserved as the validation dataset and not introduced to the ANN during training.
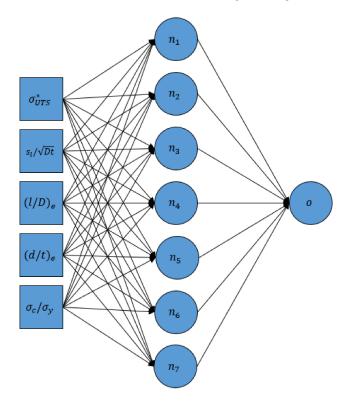


**Figure 5.** Architecture of the developed ANN.

**Table 8.** Performances of the developed ANN models based on their $R^2$ value.

| Model | No. of Neurons in Hidden 1 | $R^2$ Value |
|---|---|---|
| 1 | 1 | 0.9326 |
| 2 | 2 | 0.9358 |
| 3 | 3 | 0.9448 |
| 4 | 4 | 0.9542 |
| 5 | 5 | 0.9865 |
| 6 | 6 | 0.9854 |
| 7 | 7 | 0.9930 |
| 8 | 8 | 0.9929 |
| 9 | 9 | 0.9756 |
| 10 | 10 | 0.9686 |

Both Models 7 and 8 resulted in $R^2$ values greater than 0.99. Among the two models, Model 7 consisted of a lower number of neurons; thus, it was chosen as the ANN of choice to develop the empirical equation. The regression plot, mean squared error (MSE) that represents the best performance validation, training state, and error histogram of Model 7 are shown in Figures 6–9, respectively. Based on Figure 6, it was observed that both the dotted lines (target output) as well as the solid lines (line of best fit) in the plots overlap almost completely. This indicates that the ANN produces results that are very close to the desired output. The MSE (Figure 7) of the model was 2.0594. The R, MSE, RMSE, MAE, and MAPE values of the model for training, validation, and test phase are tabulated in Table 9. The R, MSE, RMSE, MAE, and MAPE values are calculated using Equations (8)–(12), respectively.

$$R = \frac{\sum_{i=1}^{N}(y_i - \overline{y}_i)(\hat{y}_i - \overline{\hat{y}}_i)}{\sqrt{\sum_{i=1}^{N}(y_i - \overline{y}_i)^2 \sum_{i=1}^{N}(\hat{y}_i - \overline{\hat{y}}_i)^2}} \tag{8}$$

$$MSE = \frac{1}{N}\sum_{i=1}^{N}(\hat{y}_i - y_i)^2 \tag{9}$$

$$RMSE = \sqrt{\frac{1}{N}\sum_{i=1}^{N}(\hat{y}_i - y_i)^2} \tag{10}$$

$$MAE = \frac{1}{N}\sum_{i=1}^{N}|y_i - \hat{y}_i| \tag{11}$$

$$MAPE = \frac{1}{N}\sum_{i=1}^{N}\left|\frac{y_i - \hat{y}_i}{y_i}\right| \tag{12}$$

**Table 9.** R, MSE, RMSE, MAE, and MAPE of Model 7 for training, validation, and test phase.

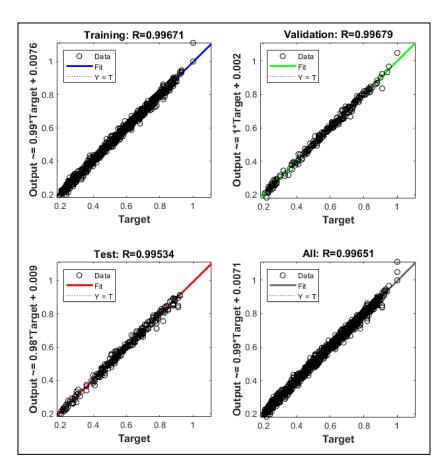| Phase | R | MSE | RMSE | MAE | MAPE (%) |
|---|---|---|---|---|---|
| Training | 0.9967 | 0.0002 | 0.0141 | 0.0499 | −7.81 |
| Validation | 0.9967 | 0.0002 | 0.0141 | 0.0537 | −6.43 |
| Test | 0.9953 | 0.0003 | 0.0173 | 0.0325 | −5.35 |

**Figure 6.** Regression plot of Model 7.
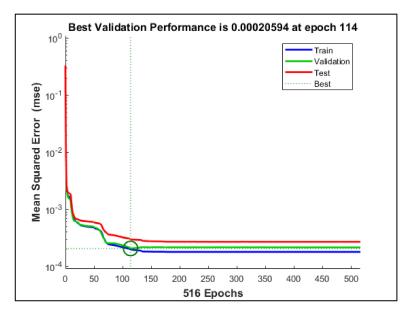


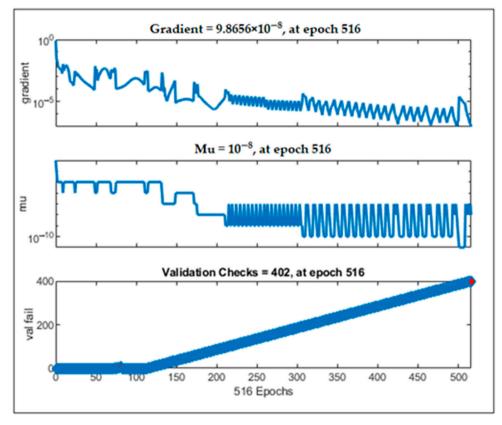**Figure 7.** Validation performance of Model 7.

**Figure 8.** Training state of Model 7.



**Figure 9.** Error histogram of Model 7.

### 3.2. Development of Empirical Equation

The weights and biases of Model 7, represented in a matrix form, are the empirical equations for the failure pressure prediction of longitudinal interacting corrosion defects subjected to internal pressure and axial compressive stress for medium- to high-toughness pipes. The steps involved in predicting the failure pressure of a corroded pipe are summarized below:

Step 1: Calculation of the normalized effective length and depth of defect.

$$(l/D)_e = \frac{l_1 + (s_1 + l_2)}{D} \tag{13}$$

$$(d/t)_e = \frac{\left(\frac{d_1 l_1 + d_2 l_2}{l_1 + (s_1 + l_2)}\right)}{t} \tag{14}$$

Step 2: Normalization of input parameters.

$$(\sigma^*_{UTS})_n = 0.01883(\sigma^*_{UTS}) - 12.52542 \tag{15}$$

$$\left(s_l/\sqrt{Dt}\right)_n = \frac{\left(s_l/\sqrt{Dt}\right)}{2} - 1 \tag{16}$$

$$(l/D)_{en} = 0.67796(l/D)_e - 1 \tag{17}$$

$$(d/t)_{en} = 2.5(d/t)_e - 1 \tag{18}$$

$$\left(\sigma_c/\sigma_y\right)_n = 2.5\left(\sigma_c/\sigma_y\right) - 1 \tag{19}$$

Step 3: Calculation of the normalized output value.

$$\begin{bmatrix} n_1 \\ n_2 \\ n_3 \\ n_4 \\ n_5 \\ n_6 \\ n_7 \end{bmatrix} = \begin{bmatrix} 0.0688 & -0.0064 & -0.0871 & -0.4542 & 0.0134 \\ 4.1762 & -0.9858 & 0.7973 & -1.0771 & 0.0326 \\ -0.0716 & -0.0491 & 1.9513 & -0.5663 & 0.1156 \\ -0.4715 & 0.0655 & -0.2014 & -0.5615 & 2.0202 \\ -0.3294 & -0.0570 & -0.0377 & 0.4955 & 0.1493 \\ 5.7885 & 0.7705 & -0.4408 & 0.8720 & -0.0218 \\ -2.6418 & -1.4969 & -0.4993 & 0.6062 & -0.0590 \end{bmatrix} \begin{bmatrix} (\sigma^*_{UTS})_n \\ (s_l/\sqrt{D/t})_n \\ (l/D)_{en} \\ (d/t)_{en} \\ (\sigma c/\sigma y)_n \end{bmatrix} + \begin{bmatrix} 0.6290 \\ -2.4461 \\ 3.0881 \\ -2.1390 \\ 0.7555 \\ 2.1732 \\ -6.3074 \end{bmatrix} \tag{20}$$

$$o_n = \begin{bmatrix} 1.8266 & 2.5203 & -3.1848 & -0.4180 & -0.8126 & -2.7257 & -2.3925 \end{bmatrix} \begin{bmatrix} a(n_1) \\ a(n_2) \\ a(n_3) \\ a(n_4) \\ a(n_5) \\ a(n_6) \\ a(n_7) \end{bmatrix} + \begin{bmatrix} -0.04112 \end{bmatrix} \tag{21}$$
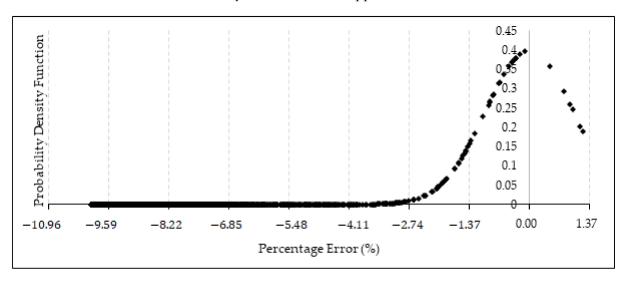
where

$$a(n_x) = \frac{2}{1 + e^{-2(n_x)}} - 1 \tag{22}$$

Step 4: Calculation of failure pressure.

$$P_f = 0.94(0.4 o_n + 0.6) P_i \tag{23}$$

### 3.3. Evaluation of the Developed Empirical Failure Pressure Assessment Method

The approach produces failure pressure estimates that are comparable to those generated using FEM, which served as the training data for Model 7. The percentage difference between the failure pressure predicted using FEM and the empirical equation for the parameters used to train the ANN is represented using a probability distribution function, as shown in Figure 10. With a standard deviation of 1.37, the percentage differences range from −10.00% to 1.22%. The confidence level that the percentage error of the predictions is less than 10.00% is 99.9%, as the errors are within eight standard deviations of the mean.

Overestimation occurred in only 0.32% of the 1843 datasets, with a maximum percentage difference of only 1.22%. Thus, this approach is reliable.



**Figure 10.** Probability distribution of the percentage error obtained using the new empirical failure pressure assessment method and FEM based on the parameters of the ANN training data.

As there is a scarcity of data on burst tests of corroded pipes subjected to combined loadings for interacting defects, FEM was used to further validate the new prediction method based on a set of arbitrary data for API 5L X52, X65, and X80 material. The parametric details, failure pressure predictions using FEM and the empirical equation, and the percentage difference between the approaches are summarized in Table 10.

**Table 10.** Comparison of the failure pressure obtained using FEA and the empirical equation for arbitrary models.

| $\sigma_{UTS}^*$ | $(s/\sqrt{Dt})$ | $(l/D)_e$ | $(d/t)_e$ | $(\sigma c/\sigma y)$ | $P_{fn,FEM}$ | $P_{fn,Eq}$ | Percentage Difference |
|---|---|---|---|---|---|---|---|
| 612.0 | 0.00 | 0.45 | 0.20 | 0.25 | 0.80 | 0.73 | −9.21 |
| 612.0 | 0.50 | 0.35 | 0.45 | 0.55 | 0.60 | 0.57 | −4.95 |
| 612.0 | 1.00 | 0.85 | 0.35 | 0.60 | 0.59 | 0.55 | −7.49 |
| 612.0 | 2.00 | 0.40 | 0.35 | 0.25 | 0.75 | 0.69 | −7.43 |
| 612.0 | 2.50 | 1.20 | 0.20 | 0.20 | 0.76 | 0.72 | −5.28 |
| 612.0 | 3.00 | 2.00 | 0.50 | 0.60 | 0.48 | 0.43 | −9.94 |
| 612.0 | 3.50 | 0.35 | 0.45 | 0.55 | 0.64 | 0.59 | −7.51 |
| 612.0 | 3.00 | 0.45 | 0.20 | 0.25 | 0.83 | 0.77 | −7.59 |
| 612.0 | 0.00 | 0.35 | 0.45 | 0.55 | 0.59 | 0.54 | −8.06 |
| 612.0 | 0.50 | 1.60 | 0.50 | 0.10 | 0.52 | 0.47 | −8.97 |
| 612.0 | 1.05 | 2.00 | 0.75 | 0.30 | 0.28 | 0.27 | −4.56 |
| 612.0 | 2.25 | 2.40 | 0.20 | 0.20 | 0.74 | 0.69 | −6.85 |
| 612.0 | 2.50 | 0.45 | 0.20 | 0.25 | 0.82 | 0.76 | -7.40 |
| 612.0 | 3.75 | 2.00 | 0.50 | 0.60 | 0.47 | 0.43 | −8.88 |
| 612.0 | 3.50 | 0.40 | 0.35 | 0.25 | 0.78 | 0.70 | −9.77 |
| 612.0 | 3.00 | 0.35 | 0.45 | 0.55 | 0.65 | 0.59 | −8.80 |
| 612.0 | 0.00 | 0.45 | 0.20 | 0.25 | 0.75 | 0.73 | −3.16 |
| 612.0 | 0.50 | 0.35 | 0.45 | 0.55 | 0.60 | 0.54 | −9.60 |

**Table 10.** *Cont.*

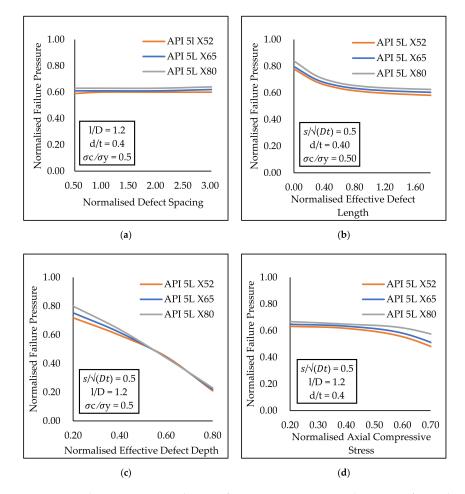| $\sigma_{UTS}^*$ | $(s/\sqrt{Dt})$ | $(l/D)_e$ | $(d/t)_e$ | $(\sigma c/\sigma y)$ | $P_{fn,FEM}$ | $P_{fn,Eq}$ | Percentage Difference |
|---|---|---|---|---|---|---|---|
| 612.0 | 1.00 | 0.85 | 0.35 | 0.60 | 0.58 | 0.54 | −6.91 |
| 629.0 | 2.00 | 1.20 | 0.20 | 0.20 | 0.78 | 0.73 | −6.23 |
| 629.0 | 2.50 | 2.00 | 0.50 | 0.10 | 0.50 | 0.45 | −9.90 |
| 629.0 | 3.00 | 2.00 | 0.50 | 0.60 | 0.35 | 0.34 | −3.32 |
| 629.0 | 3.50 | 0.40 | 0.35 | 0.25 | 0.53 | 0.48 | −8.78 |
| 629.0 | 0.00 | 0.45 | 0.20 | 0.25 | 0.84 | 0.77 | −8.88 |
| 629.0 | 0.50 | 2.40 | 0.75 | 0.30 | 0.27 | 0.26 | −5.20 |
| 629.0 | 1.00 | 0.45 | 0.20 | 0.20 | 0.80 | 0.77 | −3.60 |
| 629.0 | 2.00 | 0.35 | 0.45 | 0.25 | 0.65 | 0.62 | −4.53 |
| 629.0 | 2.50 | 0.85 | 0.35 | 0.55 | 0.58 | 0.55 | −5.30 |
| 629.0 | 3.00 | 2.00 | 0.50 | 0.60 | 0.35 | 0.34 | −3.32 |
| 629.0 | 3.25 | 0.40 | 0.35 | 0.25 | 0.55 | 0.52 | −5.22 |
| 629.0 | 0.00 | 0.40 | 0.35 | 0.25 | 0.70 | 0.69 | −1.69 |
| 629.0 | 0.50 | 1.20 | 0.20 | 0.60 | 0.69 | 0.64 | −7.47 |
| 629.0 | 1.00 | 2.00 | 0.50 | 0.60 | 0.48 | 0.45 | −6.30 |
| 629.0 | 2.00 | 2.40 | 0.75 | 0.20 | 0.23 | 0.22 | −2.61 |
| 629.0 | 2.50 | 0.40 | 0.45 | 0.10 | 0.60 | 0.56 | −6.49 |
| 629.0 | 3.50 | 0.35 | 0.45 | 0.55 | 0.28 | 0.28 | −1.22 |
| 629.0 | 3.00 | 0.45 | 0.20 | 0.25 | 0.66 | 0.61 | −7.57 |
| 629.0 | 0.00 | 0.40 | 0.35 | 0.25 | 0.76 | 0.69 | −9.45 |
| 718.2 | 0.50 | 0.45 | 0.35 | 0.25 | 0.77 | 0.71 | −8.08 |
| 718.2 | 1.00 | 0.35 | 0.20 | 0.55 | 0.79 | 0.76 | −3.72 |
| 718.2 | 2.00 | 0.85 | 0.50 | 0.10 | 0.57 | 0.52 | −8.60 |
| 718.2 | 2.50 | 0.85 | 0.50 | 0.10 | 0.45 | 0.42 | −7.11 |
| 718.2 | 3.00 | 0.40 | 0.35 | 0.25 | 0.45 | 0.45 | −0.35 |
| 718.2 | 0.00 | 2.00 | 0.75 | 0.30 | 0.28 | 0.26 | −5.92 |
| 718.2 | 0.50 | 2.40 | 0.45 | 0.20 | 0.58 | 0.54 | −6.39 |
| 718.2 | 1.00 | 0.40 | 0.35 | 0.25 | 0.76 | 0.71 | −6.64 |
| 718.2 | 2.00 | 0.45 | 0.20 | 0.55 | 0.80 | 0.75 | −6.83 |
| 718.2 | 2.50 | 0.35 | 0.50 | 0.20 | 0.46 | 0.42 | −8.37 |
| 718.2 | 3.00 | 0.40 | 0.35 | 0.25 | 0.45 | 0.45 | −0.35 |
| 718.2 | 2.35 | 0.40 | 0.35 | 0.25 | 0.64 | 0.58 | −9.77 |

Referring to Table 10, the average percentage error of the obtained results is −6.29%, suggesting that the predicted failure pressures are similar to the failure pressures determined using FEA. The percentage difference between these two methods falls between −9.90% and 0.38%. The predicted failure pressures fall within the 99.9% confidence level for true ultimate tensile strength values of 612 MPa, 629 MPa, and 718 MPa, normalized defect spacings of 0.00 to 3.00, normalized effective defect lengths of 0.00 to 2.95, normalized effective defect depths of 0.00 to 0.80, and normalized axial compressive stress of 0.00 to 0.80. In practical applications, the mechanical properties of a pipe within the same grade may vary. Even if the mechanical property of the grade varies by ±5.00%, the equation results in predictions that are within a percentage error of 13.00% without any overestimation.

## 4. Extensive Parametric Studies Using the Developed Empirical Equation

The empirical equation was utilized to conduct a parametric analysis on pipes of different grades with interacting corrosion defects to determine the effects of corrosion geometry and true ultimate tensile strength on the failure pressure of a pipe.

Based on Figure 11, it was observed that the normalized failure pressures for low-, medium-, and high-toughness materials almost overlap. This indicates that the materials exhibit the same pipe failure pattern. Referring to Figure 11a, it was observed that the normalized failure pressure increases as the normalized defect spacing is increased. This is due to the reduction in area of interaction among two defects that are longitudinally aligned. However, for a normalized effective defect length of 1.2, normalized effective defect depth of 0.4, and normalized axial compressive stress of 0.5, the increase in failure pressure is significant, with a maximum increment of 40% for API 5L X52.

As for the normalized effective defect length, for a normalized defect spacing of 0.5, normalized effective defect depth of 0.4, and normalized axial compressive stress of 0.5, the drop in failure pressure is significant for all three materials for a normalized effective defect length of 0.0 to 1.2, as depicted in Figure 11b. Beyond that, the normalized failure pressure begins to plateau. This pattern was observed to be similar for all other values of normalized defect spacing, normalized effective defect depth, and normalized axial compressive stress. Unlike normalized effective defect length, the normalized effective defect depth has a high influence on the failure pressure of a pipe with a steep drop in failure pressure as the depth increases, as illustrated in Figure 11c. This pattern was consistent for all other values of normalized defect spacing, normalized effective defect length, and normalized axial compressive stress.



**Figure 11.** Failure pressure predictions for API 5L X52, X65, and X80 pipe for multiple normalized (**a**) defect spacing; (**b**) effective defect length; (**c**) effective defect depth; (**d**) axial compressive stress.

Based on Figure 11d, for a normalized defect spacing of 0.5, normalized defect length of 1.2, and normalized defect depth of 0.4, the increase in normalized axial compressive stress resulted in a significant (a maximum of 28.33%) decrease in failure pressure for normalized axial compressive stress values of 0.4 and above. For normalized axial compressive stress values below 0.4, the drop in failure pressure was only a maximum of 2.32%. This trend was also observed for all other values of normalized defect spacing, normalized defect length, and normalized defect depth.

On the whole, all three materials exhibit the same pipe failure pattern, as the normalized failure pressure values of the pipes of different grade are almost similar. Defect depth has the most significant influence on the failure pressure of a corroded pipeline, with a maximum pressure drop of 71.22% and an average failure pressure reduction of 70.92%, followed by the defect length with a maximum pressure drop of 25.42% and average pressure reduction of 24.99%, axial compressive stress with a maximum pressure drop of 36.97% and average pressure reduction of 30.81%, and defect spacing with a maximum pressure drop of 1.69% and average pressure reduction of 1.64%. The current equation is limited only to the prescribed parameter ranges and materials. Future studies should consider more types of material, and more than two combinations of defects. To create a robust artificial neural network, more training data covering more material grades and combinations of defects should be considered during the generation of the ANN data.

## 5. Conclusions

An empirical equation to predict the failure pressure of API 5L X52, X65, and X80 pipe with longitudinally aligned interacting corrosion defects subjected to internal pressure and axial compressive stress as a function of true ultimate tensile strength, normalized defect spacing, depth and length, and axial compressive stress was developed. The new equation predicted failure pressures for these pipe grades with an $R^2$ value of 0.9930 and an error range of $-10.00\%$ to 1.22% for normalized defect spacings of 0.00 to 3.00, normalized effective defect lengths of 0.00 to 2.95, normalized effective defect depths of 0.00 to 0.80, and normalized axial compressive stress of 0.00 to 0.80.

Following that, a parametric study based on the equation was carried to demonstrate a correlation between defect geometries and failure pressure of API 5L X52, X65, and X80 pipes. It was found that the three materials exhibit the same pipe failure pattern, as the normalized failure pressure values of the pipes of different grade are almost similar. Defect depth has the most significant influence on the failure pressure of a corroded pipeline, with a maximum pressure drop of 71.22% and an average failure pressure reduction of 70.92%, followed by the defect length (maximum pressure drop of 25.42% and average pressure reduction of 24.99%), axial compressive stress (maximum pressure drop of 36.97% and average pressure reduction of 30.81%), and the defect spacing (maximum pressure drop of 1.69% and average pressure reduction of 1.64%).

**Institutional Review Board Statement:** Not applicable.

**Informed Consent Statement:** Not applicable.

**Data Availability Statement:** Not applicable.

**Conflicts of Interest:** The authors declare no conflict of interest.

## Nomenclature

| Abbreviation | Unit | Description |
| --- | --- | --- |
| ANN | - | Artificial neural network |
| DOF | - | Degree of freedom |
| FEA | - | Finite element analysis |
| FEM | - | Finite element method |
| $D$ | mm | Pipe diameter |
| $E$ | Pa | Modulus of elasticity |
| $L$ | mm | Pipe length |
| $P_f$ | Pa | Pipe failure pressure |
| $P_{fn,Eq}$ | - | Normalized pipe failure pressure obtained using the newly developed equation |
| $P_{fn,FEM}$ | - | Normalized pipe failure pressure obtained using FEM |
| $P_i$ | Pa | Pipe intact pressure |
| $d$ | mm | Defect depth |
| $d_e$ | mm | Effective defect depth |
| $d_1$ | mm | Depth of defect number 1 |
| $d_2$ | mm | Depth of defect number 2 |
| $i$ | - | Input parameter value |
| $i_{max}$ | - | Maximum input parameter value |
| $i_{min}$ | - | Minimum input parameter value |
| $i_n$ | - | Normalized input parameter value |
| $i_{n,\,max}$ | - | Normalized maximum input parameter value |
| $i_{n,\,min}$ | - | Normalized minimum input parameter value |
| $l$ | mm | Defect length |
| $l_1$ | mm | Length of defect number 1 |
| $l_2$ | mm | Length of defect number 2 |
| $n_x$ | - | Neuron in hidden layer |
| $o$ | - | Output parameter value |
| $o_{max}$ | - | Maximum output parameter value |
| $o_{min}$ | - | Minimum output parameter value |
| $o_n$ | - | Normalized output parameter value |
| $o_{n,\,max}$ | - | Normalized maximum output parameter value |
| $o_{n,\,min}$ | - | Normalized minimum output parameter value |
| $r_i$ | mm | Pipe internal radius |
| $s_c$ | mm | Circumferential defect spacing |
| $s_l$ | mm | Longitudinal defect spacing |
| $t$ | mm | Pipe wall thickness |
| $v$ | - | Poisson's ratio |
| $w$ | mm | Defect width |
| $\sigma_l$ | Pa | Axial compressive stress |
| $\sigma_{UTS}$ | Pa | Ultimate tensile strength |
| $\sigma_{UTS}^*$ | Pa | True ultimate tensile strength |
| $\sigma_y$ | Pa | Yield stress |

## References

1. Zeinoddini, M.; Arnavaz, S.; Zandi, A.P.; Vaghasloo, Y.A. Repair welding influence on offshore pipelines residual stress fields: An experimental study. *J. Constr. Steel Res.* **2013**, *86*, 31–41. [CrossRef]
2. Shuai, Y.; Zhou, D.C.; Wang, X.H.; Yin, H.G.; Zhu, S.; Li, J.; Cheng, Y.F. Local buckling failure analysis of high strength pipelines containing a plain dent under bending moment. *J. Nat. Gas. Sci. Eng.* **2020**, *77*, 103266. [CrossRef]
3. Zhang, Y.; Shuai, J.; Ren, W.; Lv, Z. Investigation of the tensile strain response of the girth weld of high-strength steel pipeline. *J. Constr. Steel Res.* **2022**, *188*, 107047. [CrossRef]
4. Arumugam, T.; Karuppanan, S.; Ovinis, M. Finite element analyses of corroded pipeline with single defect subjected to internal pressure and axial compressive stress. *Mar. Struct.* **2019**, *72*, 102746. [CrossRef]
5. Lo, M.; Karuppanan, S.; Ovinis, M. Failure Pressure Prediction of a Corroded Pipeline with Longitudinally Interacting Corrosion Defects Subjected to Combined Loadings Using FEM and ANN. *J. Mater. Sci. Eng.* **2021**, *9*, 281. [CrossRef]

6.  Kumar, S.D.V.; Karuppanan, S.; Ovinis, M. Failure Pressure Prediction of High Toughness Pipeline with a Single Corrosion Defect Subjected to Combined Loadings Using Artificial Neural Network (ANN). *Metals* **2021**, *11*, 373. [CrossRef]

7.  Belachew, C.T.; Ismail, M.C.; Karuppanan, S. Burst strength analysis of corroded pipelines by finite element method. *J. Appl. Sci.* **2011**, *11*, 1845–1850. [CrossRef]

8.  Kumar, S.D.V.; Lo, M.; Arumugam, T.; Karuppanan, S. A review of finite element analysis and artificial neural networks as failure pressure prediction tools for corroded pipelines. *Materials* **2021**, *14*, 6135. [CrossRef]

9.  Cosham, A.; Hopkins, P.; Macdonald, K.A. Best practice for the assessment of defects in pipelines—Corrosion. *Eng. Fail. Anal.* **2007**, *14*, 1245–1265. [CrossRef]

10. DNV. Recommended Practice DNV-RP-F101. Available online: https://www.dnv.com/oilgas/download/dnv-rp-f101-corroded-pipelines.html#:~{}:text=This%20recommended%20practice%20(RP)%20provides,combined%20with%20longitudinal%20compressive%20stresses (accessed on 15 April 2022).

11. Amaya-Gómez, R.; Sánchez-Silva, M.; Bastidas-Arteaga, E.; Schoefs, F.; Munoz, F. Reliability assessments of corroded pipelines based on internal pressure—A review. *Eng. Fail. Anal.* **2019**, *98*, 190–214. [CrossRef]

12. Arumugam, T.; Kasyful, M.; Mohamad, A.; Saravanan, R. Burst capacity analysis of pipeline with multiple longitudinally aligned interacting corrosion defects subjected to internal pressure and axial compressive stress. *SN Appl. Sci.* **2020**, *2*, 1201. [CrossRef]

13. Benjamin, A.C.; Freire, J.L.F.; Vieira, R.D. Analysis of pipeline containing interacting corrosion defects. *A Ser. Appl. Exp. Tech. F. Pipeline Integr.* **2007**, *31*, 74–82. [CrossRef]

14. Li, F.; Wang, W.; Xu, J.; Yi, J.; Wang, Q. Comparative study on vulnerability assessment for urban buried gas pipeline network based on SVM and ANN methods. *Process. Saf. Environ. Prot.* **2019**, *122*, 23–32. [CrossRef]

15. Silva, R.C.C.; Guerreiro, J.N.C.; Loula, A.F.D. A study of pipe interacting corrosion defects using the FEM and neural networks. *Adv. Eng. Softw.* **2007**, *38*, 868–875. [CrossRef]

16. Xu, W.Z.; Li, C.B.; Choung, J.; Lee, J.M. Corroded pipeline failure analysis using artificial neural network scheme. *Adv. Eng. Softw.* **2017**, *112*, 255–266. [CrossRef]

17. Chen, Y.; Zhang, H.; Zhang, J.; Liu, X.; Li, X.; Zhou, J. Failure assessment of X80 pipeline with interacting corrosion defects. *Eng. Fail. Anal.* **2015**, *47*, 67–76. [CrossRef]

18. Kumar, S.D.V.; Karuppanan, S.; Ovinis, M. An empirical equation for failure pressure prediction of high toughness pipeline with interacting corrosion defects subjected to combined loadings based on artificial neural network. *Mathematics* **2021**, *9*, 582. [CrossRef]

19. Tohidi, S.; Sharifi, Y.; Shari, Y. Thin-Walled Structures Load-carrying capacity of locally corroded steel plate girder ends using artificial neural network. *Thin-Walled Struct.* **2016**, *100*, 48–61. [CrossRef]

20. de Andrade, E.Q.; Benjamin, A.C.; Machado, P.R., Jr.; Pereira, L.C.; Jacob, B.P.; Carneiro, E.G.; Guerreiro, J.N.; Silva, R.C.; Noronha, D.B., Jr. Finite element modeling of the failure behavior of pipelines containing interacting corrosion defects. In Proceedings of the 25th International Conference on Offshore Mechanics and Arctic Engineering—OMAE, Hamburg, Germany, 4–9 June 2006; pp. 315–325. [CrossRef]

21. Sun, J.; Cheng, Y.F. Assessment by finite element modeling of the interaction of multiple corrosion defects and the effect on failure pressure of corroded pipelines. *Eng. Struct.* **2018**, *165*, 278–286. [CrossRef]

22. ANSYS. *ANSYS Theory Reference*; ANSYS Inc.: Canonsburg, PA, USA, 2019.

23. Wang, Y.-L.; Li, C.-M.; Chang, R.-R.; Huang, H.-R. State evaluation of a corroded pipeline. *J. Mar. Eng. Technol.* **2016**, *15*, 88–96. [CrossRef]

24. Wiesner, C.S.; Maddox, S.J.; Xu, W.; Webster, G.A.; Burdekin, F.M. Engineering critical analyses to BS 7910—The UK guide on methods for assessing the acceptability of flaws in metallic structures. *Int. J. Press. Vessel. Pip.* **2001**, *77*, 883–893. [CrossRef]

25. Cronin, D.S.; Pick, R.J. Prediction of the failure pressure for complex corrosion defects. *Int. J. Press. Vessel. Pip.* **2002**, *79*, 279–287. [CrossRef]

26. Terán, G.; Capula-Colindres, S.; Velázquez, J.C.; Fernández-Cueto, M.J.; Angeles-Herrera, D.; Herrera-Hernández, H. Failure pressure estimations for pipes with combined corrosion defects on the external surface: A comparative study. *Int. J. Electrochem. Sci.* **2017**, *12*, 10152–10176. [CrossRef]

27. Bjørnøy, O.H.; Sigurdsson, G.; Cramer, E. Residual Strength of Corroded Pipelines, DNV Test Results. In Proceedings of the Tenth (2000) International Offshore and Polar Engineering Conference, Seattle, DC, USA, 5–10 June 2000; Volume II, pp. 1–7.

28. Benjamin, A.C.; Freire, J.L.F.; Vieira, R.D.; Diniz, J.L.C.; de Andrade, E.Q. Burst Tests on Pipeline Containing Interacting Corrosion Defects. In Proceedings of the 24th International Conference on Offshore Mechanics and Arctic Engineering (OMAE 2005), Halkidiki, Greece, 12–17 June 2005; pp. 1–15.

29. Gurney, K. *An Introduction to Neural Networks an Introduction to Neural Networks*; UCL Press: London, UK, 1997.

30. Chin, K.T.; Arumugam, T.; Karuppanan, S.; Ovinis, M. Failure pressure prediction of pipeline with single corrosion defect using artificial neural network. *Pipeline Sci. Technol.* **2020**, *4*, 10–17. [CrossRef]